Volumetric Synthetic Aperture Imaging with a Piezoelectric 2-D Row-Column Probe.

Bouzari, Hamed; Engholm, Mathias; Christiansen, Thomas Lehrmann; Beers, Christopher; Lei, Anders; Stuart, Matthias Bo; Nikolov, Svetoslav Ivanov; Thomsen, Erik Vilain; Jensen, Jørgen Arendt

Published in:
Proceedings of SPIE

Link to article, DOI:
10.1117/12.2216074

Publication date:
2016

Document Version
Peer reviewed version

Volumetric Synthetic Aperture Imaging with a Piezoelectric 2-D Row-Column Probe

Hamed Bouzari[a], Mathias Engholm[b], Thomas Lehrmann Christiansen[b], Christopher Beers[c], Anders Lei[b], Matthias Bo Stuart[a], Svetoslav Ivanov Nikolov[d], Erik Vilain Thomsen[b] and Jørgen Arendt Jensen[a]

[a]Center for Fast Ultrasound Imaging, Dept. of Elec. Eng.,
Technical University of Denmark, Lyngby, Denmark
[b]Dept. of Micro- and Nanotechnology, Technical University of Denmark, Lyngby, Denmark
[c]Sound Technology, Inc., State College, Pennsylvania, USA
[d]BK Ultrasound ApS, Herlev, Denmark

ABSTRACT

The synthetic aperture (SA) technique can be used for achieving real-time volumetric ultrasound imaging using 2-D row-column addressed transducers. This paper investigates SA volumetric imaging performance of an in-house prototyped 3 MHz λ/2-pitch 62+62 element piezoelectric 2-D row-column addressed transducer array. Utilizing single element transmit events, a volume rate of 90 Hz down to 14 cm deep is achieved. Data are obtained using the experimental ultrasound scanner SARUS with a 70 MHz sampling frequency and beamformed using a delay-and-sum (DAS) approach. A signal-to-noise ratio of up to 32 dB is measured on the beamformed images of a tissue mimicking phantom with attenuation of 0.5 dB cm^{-1} MHz^{-1}, from the surface of the probe to the penetration depth of 300λ. Measured lateral resolution as Full-Width-at-Half-Maximum (FWHM) is between 4λ and 10λ for 18 % to 65 % of the penetration depth from the surface of the probe. The averaged contrast is 13 dB for the same range. The imaging performance assessment results may represent a reference guide for possible applications of such an array in different medical fields.

Keywords: 3-D ultrasound imaging, 2-D row-column addressed transducer, synthetic aperture (SA)

1. INTRODUCTION

3-D ultrasound imaging using 2-D matrix array transducers enables acquiring volumetric images of soft tissue similar to X-ray computed tomography (X-ray CT) and magnetic resonance imaging (MRI), however with a better temporal resolution. In conventional 2-D ultrasound imaging, it is required to wait for the propagation of the ultrasound pulse back and forth in the medium for each single image line. In conventional 3-D imaging, on the other hand, the number of image lines is squared, hence a quadratic reduction on the achievable frame rate is imposed. To achieve higher volume rates, i.e., higher temporal resolution, broadened (defocused) transmit beams can be used, resulting in a reduced number of emissions.[1] However, to recover the focusing capability in transmit, while using broad illuminations for a higher temporal resolution, it has been proposed to use synthetic aperture (SA) imaging, originally developed for radar detection systems.[2] By coherently combining the data acquired from successive and spatially overlapping ultrasound pulse emissions, one may retrospectively recreate a dynamic transmit focus for the full volume. Despite the intrinsic imaging difficulties that exist in 3-D ultrasound imaging with 2-D arrays, there is still a practical challenge that remains to be addressed. The number of elements in a fully addressed $N \times N$ 2-D array scales with N^2. To control the individual elements in the array, a direct connection has to be made to each element. Hereby, any delay or apodization scheme can be applied, offering maximum control and flexibility in beamforming and image processing.[3–5] To give an example, a 1-D array with a penetration depth of around 300 λ to 400 λ will for an $f_{\#} = 2$ at a depth of 200 λ require an aperture size of 64 λ to 100 λ This translates to 64 to 100 elements for a λ-pitch array, or 128 to 200 elements for a λ/2-pitch array. Using a fully addressed 2-D phased array, this would ideally correspond to an array with more than 200^2 elements. Addressing

Send correspondence to H. Bouzari, E-mail: bouzari@elektro.dtu.dk

each element individually leads to both a great practical challenge in producing the interconnections from the fabrication point of view and in sampling and real-time processing the substantial amount of data. Likewise, the small size of the elements results in lowered capacitance and henceforth increased electrical impedance mismatch between the element and the cable connecting it to the ultrasound scanner requiring preamplifiers and matching circuits in the probe handle.[6] Nevertheless, that numerous number of wires results in an impractically large cable from the transducer to the scanner.

Unlike the 1-D transducer array, where the focusing of the ultrasound wavefronts can be accomplished in only the lateral direction, in row-column addressed arrays, both orthogonal 1-D transmit and receive arrays are used for focusing separately.[7,8] This enables focusing in a 3-D volume, since every point in the space can be addressed via the two-way focusing, i.e. the product of two orthogonal transmit and receive focus lines.[9] By emulating the RF data of a 32+32 row-column addressed 2-D array, which was acquired with a 32×32 fully addressed 2-D matrix array, the imaging performance of a row-column addressed 2-D array, has been previously compared against a fully addressed 2-D array based on both simulations and measurements.[10] In this study an in-house prototyped 62+62 row-column addressed 2-D probe with integrated hardware apodization, has been used to assess the imaging performance, based on measurements on phantoms, i.e. an iron needle in a water bath facing towards the transducer as a point source, a tissue mimicking phantom, and a wire grid phantom. The imaging performance assessment results may represent a reference guide for possible applications of such an array in different medical fields.

The remainder of the paper is organized as follows: In the next section, the characterization results are presented. Section 3 presents an overview of the row-column beamforming, its advantages and disadvantages. In Section 4, a detailed overview of the equipments and the measurement setup is presented. Section 5 explains the experimental results. The final section concludes the paper with suggestions and future work.

2. PROBE MANUFACTURING AND CHARACTERIZATION

The piezoelectric (PZT) row-column array was designed and fabricated with materials and processes commonly used in commercial medical ultrasound probes. Fig. 1a shows the orientation of the row and column elements on the array. The active layer consists of a 1-3 composite of high-dielectric PZT-5H and epoxy, and to achieve a favorable ceramic aspect ratio, the composite pitch was half the array pitch. The 1-3 composite was manufactured using conventional dice and fill technique, and was ground to obtained the desired thickness of 500 µm. A metal stack of titanium tungsten, nickel vanadium, and gold in that order were then sputtered on the top and bottom surfaces of the composite for electrodes. Row and column elements were defined by scribing the top electrode in one direction and scribing the bottom electrode in the orthogonal direction. This scribe was a shallow cut made with a dicing saw resulting in a kerf of 25 µm. Separately, a high-attenuation, mechanically rigid backing block and a stack of three quarter-wavelength matching layers were fabricated. All these components were glued together, with a thin electrical interconnect layer sandwiched between the composite and the backing block. The matching layers were then diced, and the dicing was aligned with the electrode grid to reduce the mechanical coupling between adjacent elements. An initial layer of planar room temperature vulcanized (RTV) silicone was used to fill the matching layer kerfs and an electrical shield (metalized polypropylene) was then applied. The array was then mounted into a 3-D printed plastic nose piece, after which a final layer of RTV silicone was applied and leveled such that no lens effect occurred. A flexible PCB from the array was then connected to two rigid PCBs with pre-amplifiers, and a 192-channel coaxial cable was attached to the latter. The entire probe electronics and the front of the array was wrapped in a shielding foil. This shield was then connected to the shield of the coaxial cable. Finally, the two 3-D printed parts constituting the handle were assembled to complete the row-column addressed probe. The fully assembled probe is shown in Fig. 1b.

The assembled row-column probe was characterized acoustically. The pulse-echo impulse response of each element was measured at Sound Technology, Inc. (State College, PA, USA) using a XCDR II Pulse Echo Test System by emitting with one element at a time against a plane stainless steel reflector placed in DI water 25 mm from the face of the probe. Due to the available setup, the elements were actuated with a square uniform pulse having an amplitude of 50 V. The received signal was then deconvolved with the excitation pulse to yield the impulse response. In Figs. 2a and 2b, the average impulse response and its envelope are shown for the rows and columns, respectively. In this setup, the columns are the top electrodes of the PZT array, while the rows are

the bottom electrodes. Note the two extra lobes after the main lobe around −30 dB starting at times 3.1 µs and 4.5 µs. The time difference between the two is thus 1.4 µs, which corresponds to the time difference between the main lobe and the first secondary lobe. This therefore suggests reflections within the probe. The reflections correspond to the shielding foil covering the array. In Figs. 2c and 2d, the impulse response spectra are shown for the rows and columns, respectively. The center frequency and −6 dB fractional bandwidth for rows are 2.99 MHz and 82 %, and for columns are 2.99 MHz and 84 %.

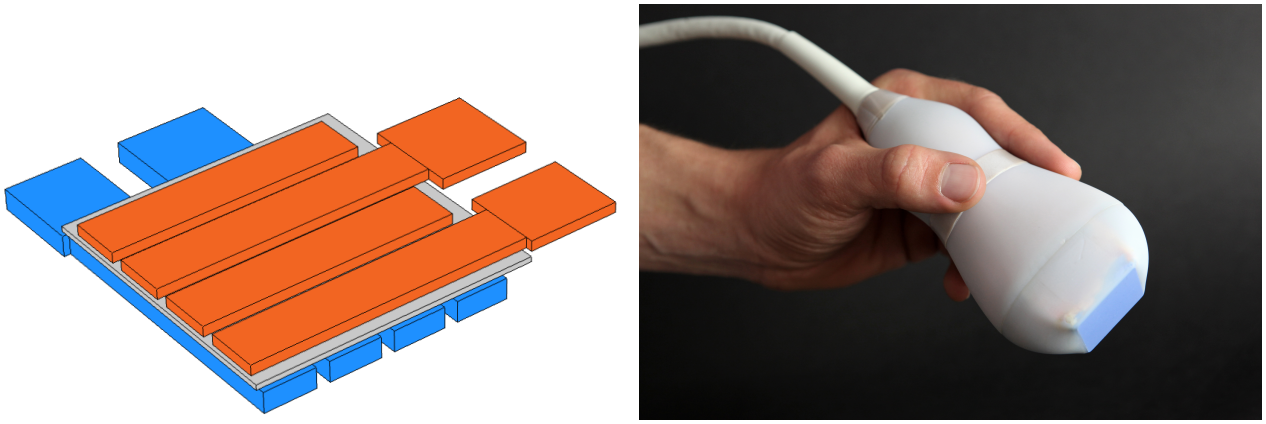

(a) (b)

Figure 1: (a) Column electrodes are shown in blue and row electrodes in orange. The PZT material is shown in gray between the top and bottom electrodes.(b) In-house prototyped 3 MHz $\lambda/2$-pitch 62+62 element piezoelectric 2-D row-column addressed probe.

3. ROW-COLUMN BEAMFORMING

Delay-and-sum beamformers usually assume the geometry of the sound sources and receivers to be points. However, by row-column addressing the elements on a 2-D matrix array, each row or column is acoustically equivalent to a line-element. Furthermore, the emitted wavefront of a line-element has the shape of a cylinder surface: it is a plane wave in the plane aligned along the line-element and a circle arc in the plane orthogonal to the line-element. Assuming the geometry of the line-elements to be points is therefore a poor approximation. A better approximation assumes the line-elements to be line-segments. When an array of line-elements is focused, the geometry of the focal zone is also a line-segment. Calculating the distances between the line-elements and a given point should therefore be calculated as the distance between a line segment and a point. For beamforming with line-element sources, the time-of-flight for the sound propagating through the media has to be calculated as (See Ref. 9 for more details):

$$t_{\text{TOF}} = \frac{\left|\vec{\mathbf{r}}_{\text{fp}_{\text{xmt}}} - \vec{\mathbf{r}}_{\text{xmt}}\right| \pm \text{d}\left(\vec{r}_{\text{p}} - \vec{\mathbf{r}}_{\text{fp}_{\text{xmt}}}\right) + \text{d}\left(\vec{\mathbf{r}}_{\text{rcv}} - \vec{r}_{\text{p}}\right)}{c}, \tag{1}$$

where $\vec{\mathbf{r}}_{\text{xmt}}$ and $\vec{\mathbf{r}}_{\text{fp}_{\text{xmt}}}$ are the vectors for each transmit line-element (along the center of the element from one end to the other) and the focal line-segment (along the focal line from one end to the other). The $\vec{r}_{\text{p}}$ is the position vector of the beamforming point p. The $\vec{\mathbf{r}}_{\text{rcv}}$ is the vector for each recieve line-element. Note that the distance between the point p and each of the transmit or recieve line-elements, follows the method to find the minimum distance between a point and a line-segment. Moreover, ± in Eq. 1, refers to whether the focal line-segment is above or below a plane orthogonal to the center line of the beam. The minimum distance between the point p

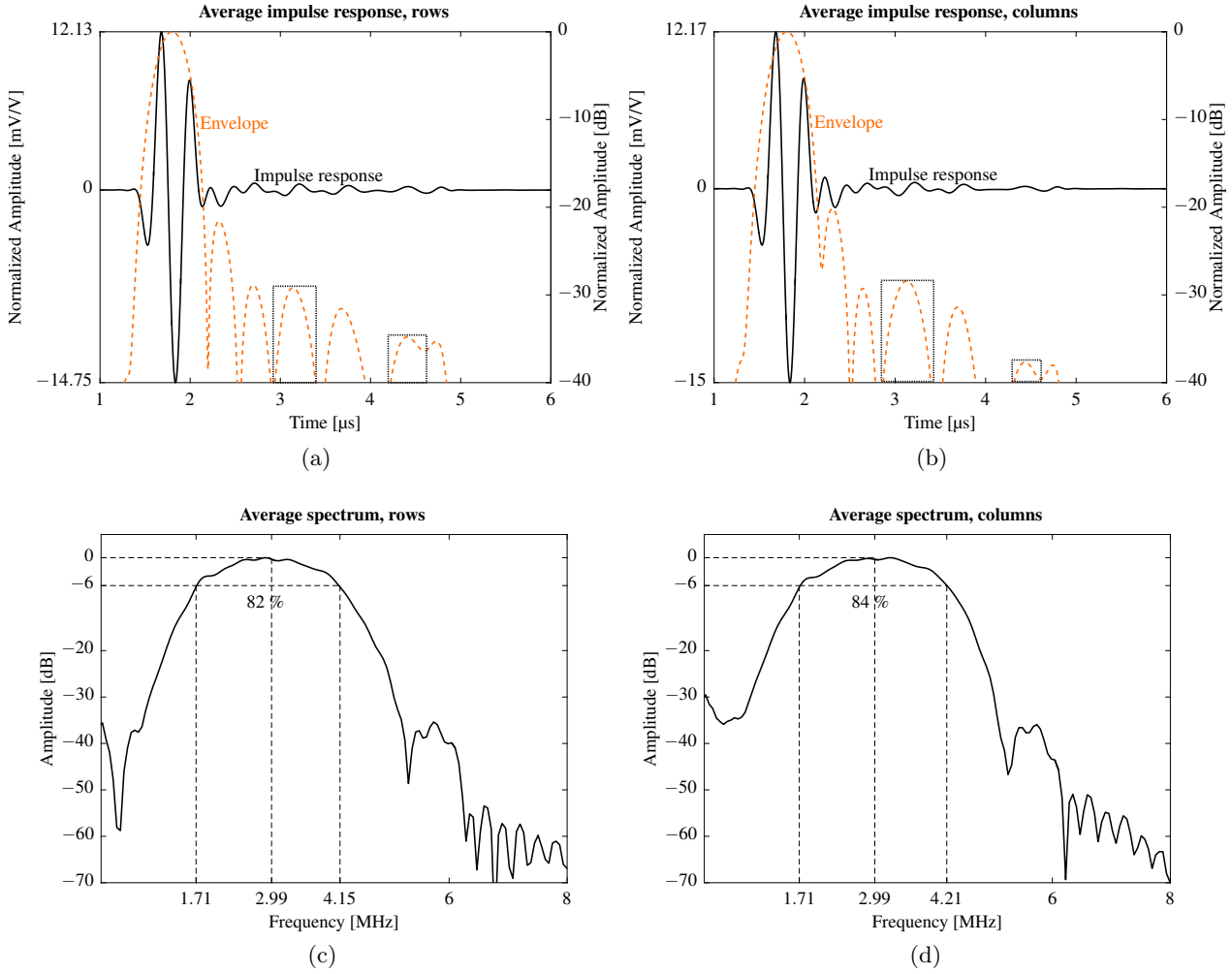

Figure 2: Average impulse response normalized to excitation voltage and its envelope for row elements (a) and column elements (b) of the probe are shown. Note the two lobes after the main lobe, indicated by dashed black rectangles, which are due to reflections from the shielding foil. The impulse response spectra are shown for the row elements in (c) and for the column elements in (d). The center frequency and $-6\,\mathrm{dB}$ fractional bandwidth are indicated in the plot.

and the line segment $\mathbf{a\vec{b}}$ is calculated as:

$$\mathrm{d}(\mathbf{ab},\mathrm{p}) = \begin{cases} \dfrac{\|\mathbf{a\vec{b}} \times \mathbf{a\vec{p}}\|}{\|\mathbf{a\vec{b}}\|} & \text{if } 0 \leq \frac{\mathbf{a\vec{p}}\cdot\mathbf{a\vec{b}}}{\|\mathbf{a\vec{b}}\|^2} \leq 1 \\ \|\mathbf{a\vec{p}}\| & \text{if } \frac{\mathbf{a\vec{p}}\cdot\mathbf{a\vec{b}}}{\|\mathbf{a\vec{b}}\|^2} < 0 \\ \|\mathbf{b\vec{p}}\| & \text{if } \frac{\mathbf{a\vec{p}}\cdot\mathbf{a\vec{b}}}{\|\mathbf{a\vec{b}}\|^2} > 1\ . \end{cases} \tag{2}$$

However, the long length of the line-elements results in prominent edge effects. These edge effects are due to the limited size of the aperture and originating from both ends of the line-element. Therefore, any excitation to a line-element generates three wavefronts: the main wavefront and two edge waves. Considering the reciprocity principle in ultrasound, every received echo also generates three pulses on the receive element.[11] Altogether there will be nine wavefronts in the pulse-echo response of a line-element. The secondary echoes after the main echo, will increase the uncertainty in the DAS beamforming process. It was shown that using hardware apodization

along each row and column element, which is different from the electronic apodization, will reduce those edge effects without altering the main echo response.[9,11] An alternative approach to decrease the amplitude of the edge echoes and also increase the spatial resolution, is beamforming by using spatial matched filtering.[8,12,13]

4. MEASUREMENT SETUPS

The volumetric data were acquired using the experimental ultrasound research scanner, SARUS.[14] The measured RF signals were beamformed using a MATLAB (MathWorks Inc., Massachusetts, USA) implemented delay-and-sum beamformer for row-column addressed arrays.[9] Table 1 lists the measurement configuration parameters. To assess the imaging performance of the PZT row-column array, several ultrasound phantoms are used. A geometrical copper wire phantom, where wires (or line targets) located at different depths have been used. A tissue mimicking phantom of comparable acoustical properties to human soft tissues also has been used. An iron needle with diameter of 300 µm facing toward the transducer and parallel to the center line of the transducer, was used as a point target in a water bath.

Table 1: Transducer's parameters and setup configuration

Center frequency	3	MHz
Pitch row(column)	270	µm
Number of rows(columns)	62	-
SA sequence (single-element emission)		
Frame rate	90	Hz
Pulse repetition frequency	5	kHz
Emissions per frame	62	-
Number of active elements	124	-
Scan depth (max range)	14	cm
Emission cycles	2	-
Tx apodization	Hamming	-
Rx apodization	Hamming	-
Sampling frequency	70	MHz

Table 2: FWHM and cystic resolution measurements

	Measurement	Simulation	
$R_{6\text{dB}}$	0.51	0.38	mm
$R_{12\text{dB}}$	0.82	0.61	mm
$R_{20\text{dB}}$	1.33	0.9	mm
Axial FWHM	532.5	325	µm
Azimuth FWHM	1375	1030	µm
Elevation FWHM	1312	1030	µm

5. RESULTS AND DISCUSSION

Figure 3, shows the measured and simulated 3-D point spread function (PSF) of SA in a water bath. In this study, Field II[16,17] simulations are used to validate the measured results. The full-width at half-maximum (FWHM)

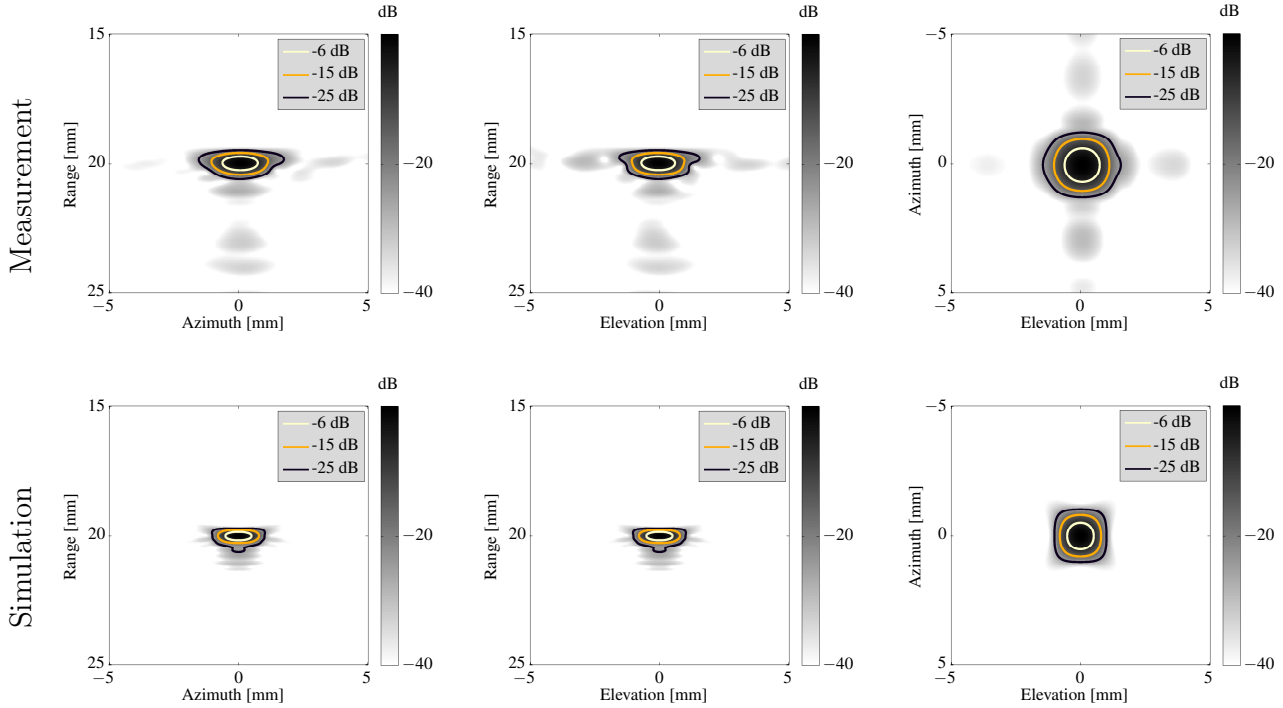

Figure 3: Volumetric imaging of a needle pointing towards the transducer using the developed probe and comparing to its simulated 3-D PSF at the same location. Three cross-planes (azimuth, elevation, and C-plane) are shown from a volume of 10 mm×10 mm×10 mm at a dynamic range of 40 dB. The origin corresponds to the center of the transducer surface. Note the "ghost" echoes, which are due to the extra reflections in the impulse response seen in Fig. 2a and Fig. 2b. The full-width at half-maximum (FWHM) and the side lobe energy metrics (cystic resolution[15]), for the measured and simulated 3-D PSFs are listed in Table 2.

and the side lobe energy metrics (cystic resolution[18]), for the measured and simulated PSFs are listed in Table 2. Lateral FWHM values are larger compared to 1-D transducers with the same lateral size. For row-column addressed 2-D arrays, the transmit focusing and receive focusing are not taking place in the same plane, but instead in planes perpendicular to each other and this affects the PSF size. Figs. 4 and 5 show the volumetric images of a tissue mimicking cyst phantom and a wire grid phantom. It is worth mentioning that in the wire grid image, the size of the line spread functions (LSF) is getting larger and therefore around the depth of 90 mm, it is not possible to discriminate individual wires from each other. Once more, due to one-way focusing, the lateral and elevation resolution as a function of depth, decreases faster than 1-D transducers of equivalent size. The cylindrical cyst regions are visible in the tissue mimicking phantom in Fig. 4. The contrast to noise ratio (CNR) over an anechoic cylindrical cyst region with diameter of 8 mm at the depth of 27 mm, (Fig. 4) on a tissue mimicking phantom with attenuation coefficient of 0.5 dB MHz^{-1} cm^{-1}, was 0.54, compared to the background. The CNR was calculated as $|\mu_{\text{bck}} - \mu_{\text{cyst}}| \,/\, \sqrt{(\sigma^2_{\text{bck}} + \sigma^2_{\text{cyst}})/2}$, where μ_{bck} and μ_{cyst} are mean gray level of background and cyst, σ^2_{bck} and σ^2_{cyst} are variances of gray levels within background and lesion, respectively. Fig. 6 shows the SNR of the SA imaging single-element sequence on a tissue mimicking phantom with an attenuation coefficient of 0.5 dB MHz^{-1} cm^{-1}. A maximum SNR of 32 dB is measured and the penetration depth is about 300λ for SNR=0 dB.

6. CONCLUSION AND PERSPECTIVES

In this study, the imaging performance of a piezoelectric 2-D row-column addressed probe for real-time 3-D synthetic aperture imaging was presented based on phantom measurements from the experimental ultrasound

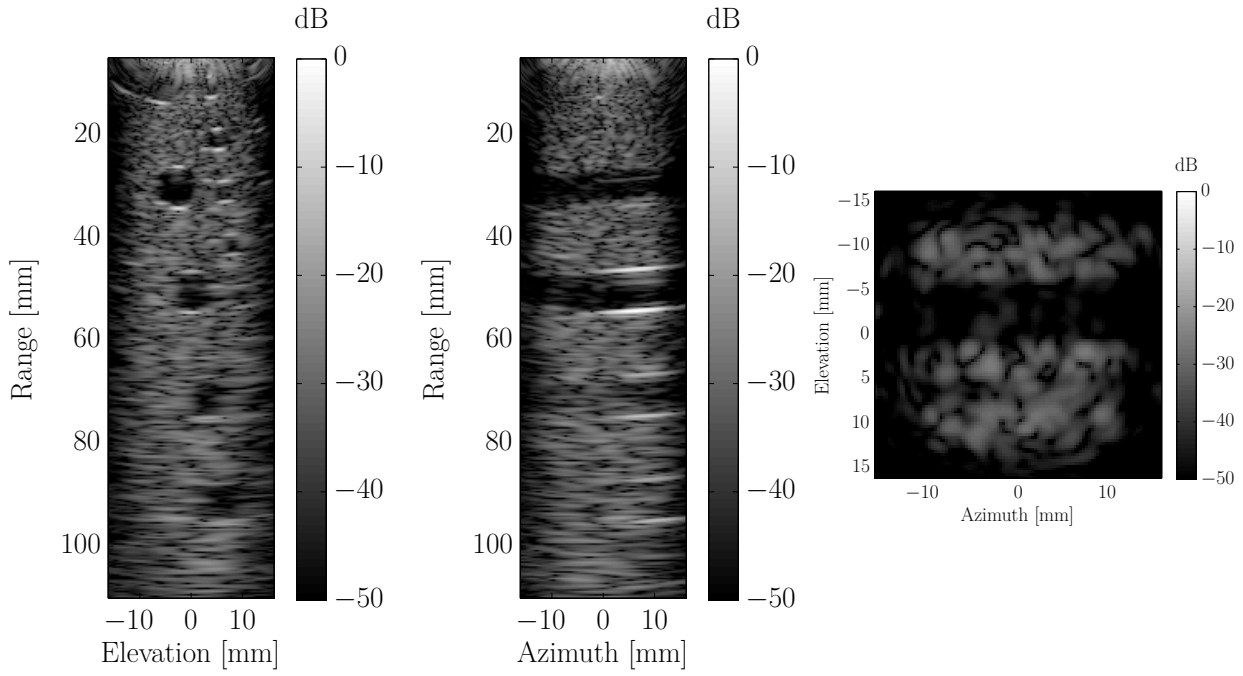

Figure 4: Volumetric imaging of a hollow cyst phantom using the developed probe. Three cross-planes (elevation, azimuth, and C-plane) are shown from a beamformed volume of 30 mm×30 mm×100 mm at a dynamic range of 50 dB. The origin corresponds to the center of the transducer surface. The C-plane was at 30 mm depth.

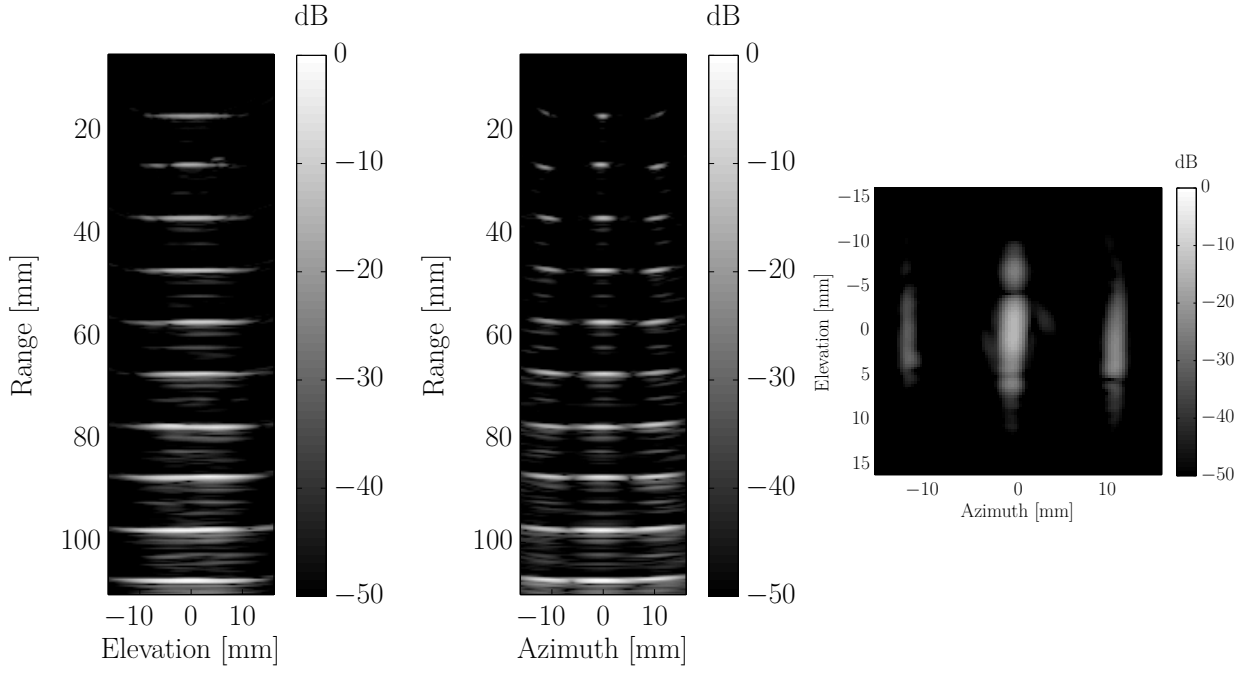

Figure 5: Volumetric imaging of a wire phantom using the developed probe. Three cross-planes (elevation, azimuth, and C-plane) are shown from a beamformed volume of 30 mm×30 mm×100 mm at a dynamic range of 50 dB. The origin corresponds to the center of the transducer surface. The spacing between wires is 10 mm. The C-plane was at 26 mm depth.

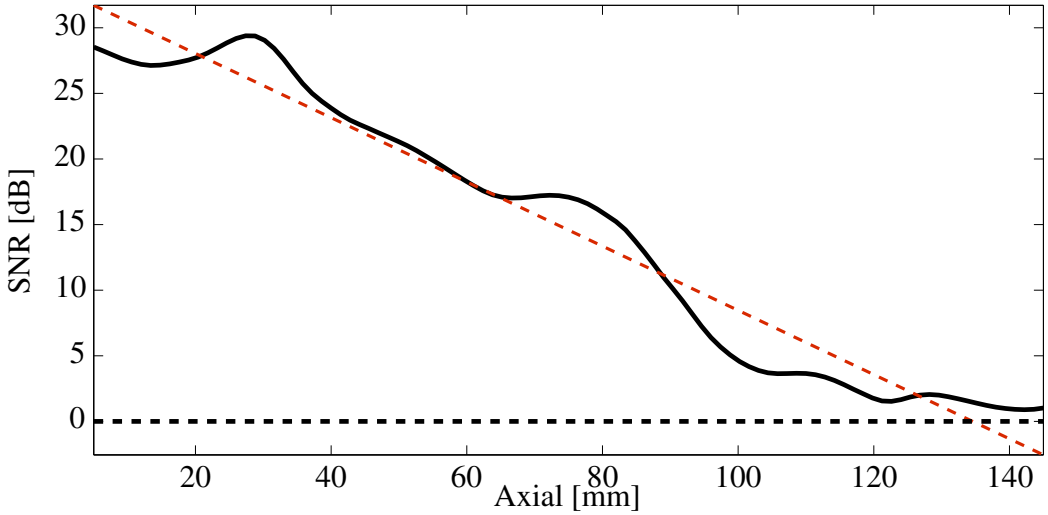

Figure 6: The black line shows the SNR on a tissue mimicking phantom with attenuation of $0.5\,\mathrm{dB\,cm^{-1}\,MHz^{-1}}$, along the center line over 15 measurements. The dashed red line shows the linearly interpolated SNR curve. The penetration depth of about 14 cm can be observed, where the curve crosses 0 dB (black dashed line).

scanner SARUS. It was shown that using synthetic aperture imaging on a 2-D row-column addressed transducer array a high volume rate imaging at a low cost could be achieved. Although 3-D visualizing gives the clinician a better insight for possible pathology and medical treatments, having a high volume rate makes it possible to capture dynamics, which otherwise cannot be detected by other 3-D imaging modalities. On the other hand, by row-column addressing, larger arrays are possible to build, which seemed impractical until recently. The direct benefit of a larger aperture size is to have a higher resolution, which makes it suitable for abdominal scans. The imaging performance results, which presented in this paper may represent a reference guide for possible applications of row-column addressed arrays in different medical fields.

REFERENCES

[1] Shattuck, D. P., Weinshenker, M. D., Smith, S. W., and von Ramm, O. T., "Explososcan: A parallel processing technique for high speed ultrasound imaging with linear phased arrays," *J. Acoust. Soc. Am.* **75**, 1273–1282 (1984).

[2] Burckhardt, C. B., Grandchamp, P.-A., and Hoffmann, H., "An experimental 2 MHz synthetic aperture sonar system intended for medical use," *IEEE Trans. Son. Ultrason.* **21**, 1–6 (January 1974).

[3] Turnbull, D. H. and Foster, F. S., "Beam steering with pulsed two-dimensional transducer arrays," *IEEE Trans. Ultrason., Ferroelec., Freq. Contr.* **38**, 320–333 (July 1991).

[4] Karaman, M., Li, P. C., and O'Donnell, M., "Synthetic aperture imaging for small scale systems," *IEEE Trans. Ultrason., Ferroelec., Freq. Contr.* **42**, 429–442 (1995).

[5] Thomenius, K. E., "Evolution of ultrasound beamformers," in [*Proc. IEEE Ultrason. Symp.*], **2**, 1615–1621 (1996).

[6] Karadayi, K., Managuli, R., and Kim, Y., "Three-dimensional ultrasound: From acquisition to visualization and from algorithms to systems," *IEEE Rev Biomed Eng* **2**, 23–39 (2009).

[7] Démoré, C. E. M., Joyce, A., Wall, K., and Lockwood, G., "Real-time volume imaging using a crossed electrode array," *IEEE Trans. Ultrason., Ferroelec., Freq. Contr.* **56**(6), 1252–1261 (2009).

[8] Yen, J. T., "Beamforming of sound from two-dimensional arrays using spatial matched filters," *J. Acoust. Soc. Am.* **134**(5), 3697–704 (2013).

[9] Rasmussen, M. F., Christiansen, T. L., Thomsen, E. V., and Jensen, J. A., "3-D imaging using row–column-addressed arrays with integrated apodization — Part I: Apodization design and line element beamforming," *IEEE Trans. Ultrason., Ferroelec., Freq. Contr.* **62**(5), 947–958 (2015).

[10] Rasmussen, M. F. and Jensen, J. A., "3-D ultrasound imaging performance of a row-column addressed 2-D array transducer: A measurement study," in [*Proc. IEEE Ultrason. Symp.*], 1460–1463 (July 2013).

[11] Christiansen, T. L., Rasmussen, M. F., Jensen, J. A., and Thomsen, E. V., "Row-column addressed 2-D CMUT arrays with integrated apodization," in [*Proc. IEEE Ultrason. Symp.*], 600–603 (2014).

[12] Jensen, J. A. and Gori, P., "Spatial filters for focusing ultrasound images," in [*Proc. IEEE Ultrason. Symp.*], 1507–1511 (2001).

[13] Bouzari, H., Engholm, M., Christiansen, T. L., Stuart, M. B., Nikolov, S. I., Thomsen, E. V., and Jensn, J. A., "Volumetric ultrasound imaging with row-column addressed 2-d arrays using spatial matched filter beamforming," in [*Proc. IEEE Ultraso. Symp.*], 1–4, IEEE (2015).

[14] Jensen, J. A., Holten-Lund, H., Nilsson, R. T., Hansen, M., Larsen, U. D., Domsten, R. P., Tomov, B. G., Stuart, M. B., Nikolov, S. I., Pihl, M. J., Du, Y., Rasmussen, J. H., and Rasmussen, M. F., "SARUS: A synthetic aperture real-time ultrasound system," *IEEE Trans. Ultrason., Ferroelec., Freq. Contr.* **60**(9), 1838–1852 (2013).

[15] Rasmussen, M. F. and Jensen, J. A., "Comparison of 3-D synthetic aperture phased array ultrasound imaging with parallel beamforming," *IEEE Trans. Ultrason., Ferroelec., Freq. Contr.* **61**(10), 1638–1650 (2014).

[16] Jensen, J. A. and Svendsen, N. B., "Calculation of pressure fields from arbitrarily shaped, apodized, and excited ultrasound transducers," *IEEE Trans. Ultrason., Ferroelec., Freq. Contr.* **39**, 262–267 (1992).

[17] Jensen, J. A., "Field: A program for simulating ultrasound systems," *Med. Biol. Eng. Comp.* **10th Nordic-Baltic Conference on Biomedical Imaging, Vol. 4, Supplement 1, Part 1**, 351–353 (1996).

[18] Ranganathan, K. and Walker, W. F., "Cystic resolution: A performance metric for ultrasound imaging systems," *IEEE Trans. Ultrason., Ferroelec., Freq. Contr.* **54**(4), 782–792 (2007).